Elastohydrodynamic Suppression of Free-Surface Instabilities in Annular Liquid Film Flow Outside Wires and Inside Tubes

Aashish Jain and V. Shankar*

Department of Chemical Engineering, Indian Institute of Technology, Kanpur 208 016, India

The linear stability of gravity-driven annular liquid film flow outside wires and inside tubes is analyzed when the rigid surface is replaced by a deformable (neo-Hookean) solid wall. On a rigid surface, an annular liquid thread becomes unstable due to a Rayleigh-type capillary instability even in the absence of flow. In the presence of flow, the annular liquid film becomes unstable due to a flow-driven, free-surface instability, which occurs over and above the curvature-induced capillary instability. In this paper, a low-wavenumber perturbation analysis is first used to elucidate the effect of wall deformability on the free-surface instability. It is shown that the free-surface instability is completely stabilized in the low-wavenumber limit when the wall is made sufficiently deformable. A numerical method is subsequently used to determine the stability of the system at arbitrary wavenumbers. Results from the numerical solution reveal that the prediction of instability suppression at low wavenumbers extends to finite wavenumbers as well. However, as the solid wall is made deformable even further, the free surface is destabilized at finite wavenumbers by the deformability; in addition, the liquid−solid interface could also become unstable when the solid deformability becomes high. It is demonstrated, however, that there is a sufficient range of shear modulus of the solid where the annular flow is stable at all wavenumbers. The results of this study have implications in wire-coating operations, as well as in biological settings such as closure of lung airways.

1. Introduction

Flow of liquid films down a cylindrical solid surface under the influence of gravity is frequently encountered in a wide class of technological applications such as wire-coating processes,[1] as well as in biological settings such as flow in lung airways.[2,3] Such film flows have a free surface, and hence, surface tension forces become important in addition to viscous forces and gravitational forces. An important issue in such flows is the possibility of obtaining a smooth, uniform liquid coating on the outer or inner side of a cylindrical surface. However, it is well-known[4,5] that cylindrical liquid threads are prone to curvature-induced capillary instabilities even in the absence of any flow. With the presence of flow, gravity-driven flows of planar liquid films are subjected to a flow-induced instability, as shown first by Benjamin[6] and Yih.[7] This flow-induced, free-surface instability persists even when the geometry of the surface changes from planar to cylindrical. Thus, for liquid flow on the outer or inner side of a cylindrical surface, two different mechanisms, one curvature-induced and the other flow-induced, act together to destabilize the free surface. This free-surface instability manifests as varicose-shaped ripples on the free surface, which travel down the flow. Such unstable flows with a nonuniform free surface can either be beneficial or detrimental, depending on the physical application. These ripples could be beneficial in some industrial applications because they improve the heat- and mass-transfer characteristics in film flows. In other applications such as coating by extrusion or air flow in lungs, such instabilities are undesirable for the following reasons. Instabilities at the interface affect product quality in extrusion-based coating processes, while in air flow inside small lung airways, the instability of the liquid film present on the inner side of the lung airways could lead to closing of the small airways.[2] In this paper, we propose and evaluate the feasibility of using deformable elastomeric coatings on the rigid surface in order to suppress the free-surface instability. In the remainder of this Introduction, we briefly review the relevant literature and place the present work in perspective.

It is well-known since the classic works of Plateau and Rayleigh,[4,5] that a stationary cylindrical liquid jet (of radius R) is unstable in the inviscid limit to varicose-shaped perturbations to the free surface, when the wavelength of the perturbations is larger than the perimeter $2\pi R$ of the jet. For such perturbations, the destabilizing pressure forces due to radial curvature overcome the stabilizing pressure forces due to axial curvature, thereby causing the breakup of the liquid jet into droplets. The unstable mode with the largest growth rate has a wavelength $\lambda \approx 2\pi R/0.7$ a little larger than the perimeter of the jet. When a stationary viscous jet is considered,[4] a similar instability is found, but with the difference that the maximum growth rate occurs for perturbations with infinitely large wavelengths. This classical jet instability problem has been extended by several authors to the technologically relevant application of wire or fiber coating, where there is an annular liquid thread coating the outer surface of a solid cylinder. Goren[8] analyzed the problem for a stationary annular liquid film and found a capillary instability similar to the classical Rayleigh instability, which agreed well with experimental results. A number of subsequent studies[9−12] focused on the effect of flow on the free-surface instability on a annular film coated on a wire. The presence of flow gives rise to an additional mode of instability, which is present even in the case of a planar gravity-driven liquid film flow.[7] Thus, flow further destabilizes an annular liquid film on the outer or inner surface of a cylinder. However, Russo and Steen[12] showed that when there is an imposed shear at the free surface, it is possible to stabilize the instability at the free surface at any wavenumber. It is also possible that after the onset of linear instability, nonlinear effects can saturate the instability, which can prevent the film from rupturing into droplets.[1]

Recently, it was shown that soft, deformable solid walls could suppress the instability at the free surface of gravity-driven

* To whom correspondence should be addressed. E-mail: vshankar@iitk.ac.in. Tel: +91-512-2597377. Fax: +91-512-2590104.

10.1021/ie701771m CCC: $40.75
Published on Web 07/08/2008

planar film flow.[13,14] This stabilization occurs because of the elastohydrodynamic coupling between fluid flow and solid deformation: the deformation in the solid induced by the flow affects the flow itself and leads to a secondary flow that opposes the instability. In this work, we extend those studies to the cylindrical geometry, where we consider both film flow outside (wire coating) and inside (tube flow) of a cylinder, by making the rigid cylindrical wall deformable. The latter configuration may naturally arise in the case of lung airways,[2] where the conveying vessel is deformable and is coated on the inside with a liquid film through which there is air flow. The main motivation for the present work is to examine whether the curvature-induced capillary instability of an annular film could also be suppressed by the deformability of the solid, apart from the flow-induced free-surface instability.

The rest of this paper is structured as follows: we set up the governing equations for the problem and formulate the linearized stability equations in section 2. A low-wavenumber perturbation analysis is carried out in section 3 in order to elucidate the effect of deformability of the solid on the free-surface mode. A numerical method is used to continue the low-wavenumber results to arbitrary finite wavenumbers in section 4, and the salient conclusions are discussed in section 5.

2. Problem Formulation

The system we consider consists of the flow of an incompressible Newtonian liquid past an incompressible and impermeable deformable solid down the outer and inner walls of a circular cylinder as shown respectively in Figures 1 and 2, respectively. The deformable solid is strongly bonded to the rigid wall at $r^* = r_0$ and is characterized by a shear modulus G and thickness L_0. The liquid layer is in contact with a passive gas and occupies a region $r_0 + L_0 \le r^* \le r_0 + L_0 + h_0$ for outside flow and $r_0 - L_0 \le r^* \le r_0 - L_0 - h_0$ for inside flow. The densities of liquid and solid are assumed to be equal, without loss of generality. In what follows, we denote dimensional variables with an asterisk and nondimensional variables without any superscript. Various physical quantities are nondimensionalized by using the following scales: lengths and displacements with h_0 (fluid film thickness), velocities with the free-surface velocity V of the laminar base flow, time with h_0/V, pressures and stresses with $\mu V/h_0$. Here, the density of the fluid is denoted by ρ, viscosity by μ, and g is the gravitational acceleration. The nondimensional equations governing the dynamics of the fluid are the mass and momentum conservation equations:

$$\nabla \cdot \mathbf{v} = 0 \tag{1}$$

$$Re\left[\frac{\partial \mathbf{v}}{\partial t} + \mathbf{v} \cdot \nabla \mathbf{v}\right] = \nabla \cdot \mathbf{T} + \hat{\mathbf{g}} \tag{2}$$

Here, $\mathbf{v}$ represents the velocity field in the liquid, $\hat{\mathbf{g}}$ is the unit vector pointing in the direction of gravity, $Re = \rho V h_0/\mu$ is the Reynolds number, $\mathbf{T} = -p_f\mathbf{I} + \tau$ is the total stress tensor in the fluid, which is a sum of an isotropic pressure $-p_f\mathbf{I}$ and the extra-stress tensor $\tau = [\nabla\mathbf{v} + (\nabla\mathbf{v})^T]$.

While many theoretical studies in the area of flow past deformable solid media have used the linear elastic model for describing the deformation in the solid, recently Gkanis and Kumar[15,16] pointed out that the linear elastic model is strictly valid only when the strain in the solid layer is small and that appropriate modifications must be made at finite deformations in order to obey the principle of material frame indifference.[17,18] In lieu of the linear elastic solid, they suggested the use of a neo-Hookean model, which is a frame-invariant generalization of the Hookean model for solids and is applicable for finite and large deformations[19] typically encountered in soft solid materials such as elastomers. The neo-Hookean solid yields a first-normal stress difference in the base state, and the discontinuity of this normal stress in the base state at the liquid−solid interface was shown to give rise to a shortwave instability, which is absent in linear viscoelastic solids. In this study, therefore, we employ the neo-Hookean constitutive relation to determine the solid deformation. Here, we assume the solid to be incompressible. The deformation field satisfies the momentum and mass conservation equations, and the nondimensional equations governing the deformation in neo-Hookean solid are given as[17,18]

$$\det(\mathbf{F}) = 1 \tag{3}$$

$$Re\left[\frac{\partial^2 r}{\partial t^2}\right]_R = \nabla_R \cdot P + \hat{g} \tag{4}$$

Here, $\mathbf{P}$ is the first Piola−Kirchhoff tensor, $\mathbf{F}$ is the deformation gradient tensor. The deformation gradient tensor in the cylindrical coordinate system is defined as $\mathbf{F} = \nabla_R \mathbf{r}$, where $\mathbf{r} \equiv (u_r, u_\theta, u_z)$ represents the position vector of a material particle in the current configuration of the neo-Hookean solid. The capital letter $\mathbf{R} = (R, \Theta, Z)$ denotes the spatial coordinates in reference configuration, and hence, subscript R in eq4 indicates a gradient with respect to reference coordinates. For the liquid, (r, θ, z) coordinate system is used and this coordinate system coincides with the reference coordinate system (R, Θ, Z) for neo-Hookean solid. The first Piola−Kirchhoff stress tensor is related to the usual Cauchy stress tensor by $\mathbf{P} = \mathbf{F}^{-1} \cdot \boldsymbol{\sigma}$. The Cauchy stress tensor for neo-Hookean solid is given by[19]

$$\sigma = -p_s\mathbf{I} + \frac{1}{\Gamma}(\mathbf{F} \cdot \mathbf{F}^T) \tag{5}$$

where p_s is the pressure in neo-Hookean solid, and $\Gamma \equiv V\mu/(GR)$ is the nondimensional parameter characterizing the deformability of the solid layer.

The conditions at the free surface ($r = S \pm L \pm 1$) are the kinematic condition for evolution of free surface and the tangential and normal stress balances. Here $S(= r_0/h_0)$ and $L(= L_0/h_0)$ are the nondimensional radius and solid thickness, respectively. A positive sign represents outside flow while negative sign represents inside flow. The tangential stresses at the free surface are zero and normal stress in the liquid is balanced by the hydrostatic pressure in the gas adjacent to it.

$$\partial_t h + v_z \partial_z h = v_r \tag{6}$$

$$\mathbf{n} \cdot \mathbf{T} \cdot \mathbf{t} = 0 \tag{7}$$

$$\mathbf{n} \cdot \mathbf{T} \cdot \mathbf{n} + \Sigma_f(\nabla \cdot \mathbf{n}) = 0 \tag{8}$$

where, h is the free surface position, $\mathbf{n}$ and $\mathbf{t}$ are the normal and tangential unit vectors to the free surface, respectively, and $\Sigma_f = \gamma_f/\mu V$ is the nondimensional surface tension parameter at the free surface, with γ_f being the dimensional surface tension at the free surface. At the liquid−solid interface ($r = S \pm L$), the velocities and stresses in liquid and solid layers are continuous. The condition of velocity continuity is given as

$$\mathbf{v} = \frac{\partial \mathbf{r}}{\partial t} \tag{9}$$

The normal and tangential stress balances are given by

$$\mathbf{n} \cdot \mathbf{T} \cdot \mathbf{t} = \mathbf{n} \cdot \sigma \cdot \mathbf{t} \tag{10}$$

$$\mathbf{n} \cdot \mathbf{T} \cdot \mathbf{n} - \mathbf{n} \cdot \sigma \cdot \mathbf{n} = \Sigma_i(\nabla \cdot \mathbf{n}) \tag{11}$$

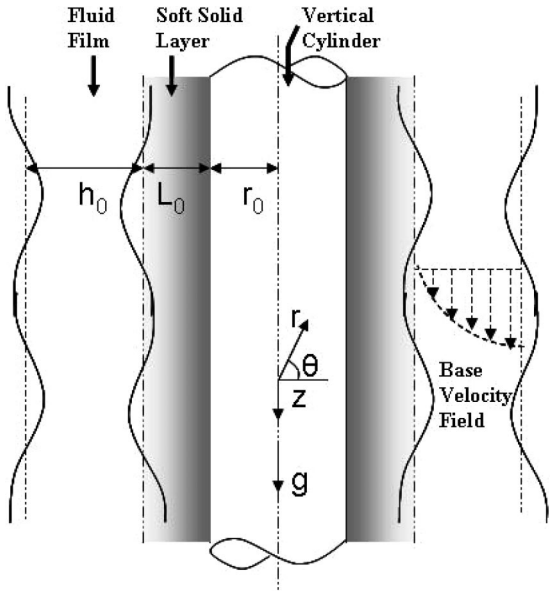

Figure 1. Schematic diagram of the configuration and coordinate system, when there is a flow outside a cylindrical geometry lined with a deformable solid layer. The wavy lines depict the perturbed interfaces.

Here, **n** and **t** are the normal and tangential unit vectors for liquid−solid interface, and $\Sigma_i = \gamma_i/\mu V$ is the nondimensional surface tension parameter, with γ_i being the dimensional liquid−solid interface tension. We have used the same symbols **n** and **t** for the unit normal and tangent vectors for both the free surface and liquid−solid interface. At the rigid surface ($r = S$) zero displacement condition is satisfied: $\mathbf{r} = \mathbf{R}$.

2.1. Base State. The laminar base state of the present system consists of unidirectional flow of the liquid in z direction due to gravity. The solid layer is at rest in this steady state with a nonzero displacement in the z direction due to liquid shear stress at the interface. Both the gas−liquid and liquid−solid interfaces remain cylindrical and uniform in the base state. The dimensional velocity scale V (i.e., the free-surface velocity of the laminar flow) is given by

$$V = \frac{\rho g}{4\mu}\left\{-h_0(h_0 + 2(L_0 \pm r_0)) + 2(r_0 \pm L_0 \pm h_0)^2 \times \log\left[\frac{r_0 \pm L_0 \pm h_0}{r_0 \pm L_0}\right]\right\} \quad (12)$$

The nondimensional velocity profile and pressure distribution in liquid layer are given as

$$\bar{v}_z = \frac{\left[(S \pm L)^2 - r^2 + 2(S \pm L \pm 1)^2 \log\left(\frac{r}{S \pm L}\right)\right]}{-(1 + 2L \pm 2S) + 2(1 + L \pm S)^2 \log\left(\frac{S \pm L \pm 1}{S \pm L}\right)} \quad (13)$$

$$\bar{v}_r = 0 \quad (14)$$

$$\bar{p} = \frac{\pm\Sigma_f}{S \pm L \pm 1} \quad (15)$$

The Lagrangian position of a material particle and pressure field in the neo-Hookean solid are given by:

$$\bar{u}_z = Z + \frac{\Gamma\left[S^2 - r^2 + 2(S \pm L \pm 1)^2 \log\left(\frac{r}{S}\right)\right]}{-(1 + 2L \pm 2S) + 2(1 + L \pm S)^2 \log\left(\frac{S \pm L \pm 1}{S \pm L}\right)} \quad (16)$$

$$\bar{u}_r = R \quad (17)$$

$$\bar{p}_s = \frac{1}{\Gamma} \pm \left(\frac{\Sigma_i}{S \pm L} + \frac{\Sigma_f}{S \pm L \pm 1}\right) \quad (18)$$

2.2. Linear Stability Analysis. A temporal linear stability analysis is performed in order to determine the stability of the present annular configuration. All the dynamical quantities (velocities, displacement, pressure, etc.) are perturbed about the base state and are substituted in the governing equations. The resulting equations are then linearized to obtain a set of equations in terms of perturbation quantities. The perturbations are expanded in the form of Fourier modes,

$$f' = \tilde{f}(r)\ \exp[ik(z - ct)] \quad (19)$$

where, f' is the perturbation to any physical variable, k is the (real) wavenumber of perturbations, c is the complex wavespeed, and $\tilde{f}(r)$ is the complex amplitude function of the disturbance. For neo-Hookean model, $z$and r are replaced by Z and R, respectively. The imaginary part of complex wavespeed determines the stability of the system: If $c_i > 0$, the initially small perturbations will grow with time and the flow is considered unstable. If it is negative, the disturbances will die down and flow is considered to be temporally stable.

When the above form of perturbations is substituted in the linearized perturbation equations and boundary conditions, one obtains a set of equations in terms of amplitude functions and wavespeed, c, that governs the stability of the system. Thus, the governing equations for liquid layer are:

$$\frac{d\tilde{v}_r}{dr} + \frac{\tilde{v}_r}{r} + ik\tilde{v}_z = 0 \quad (20)$$

$$Re[ik(\bar{v}_z - c)\tilde{v}_z + (d_r\bar{v}_z)\tilde{v}_r] = -ik\tilde{p} + \frac{d^2\tilde{v}_z}{dr^2} + \frac{1}{r}\frac{d\tilde{v}_z}{dr} - k^2 v_z \quad (21)$$

$$Re[ik(\bar{v}_z - c)\tilde{v}_r] = -\frac{d\tilde{p}}{dr} + \frac{d^2\tilde{v}_r}{dr^2} + \frac{1}{r}\frac{d\tilde{v}_r}{dr} - \left(k^2 + \frac{1}{r^2}\right)\tilde{v}_r \quad (22)$$

The above equations can be combined to give a single fourth-order, Orr-Sommerfeld like equation for $\tilde{v}v_r$:

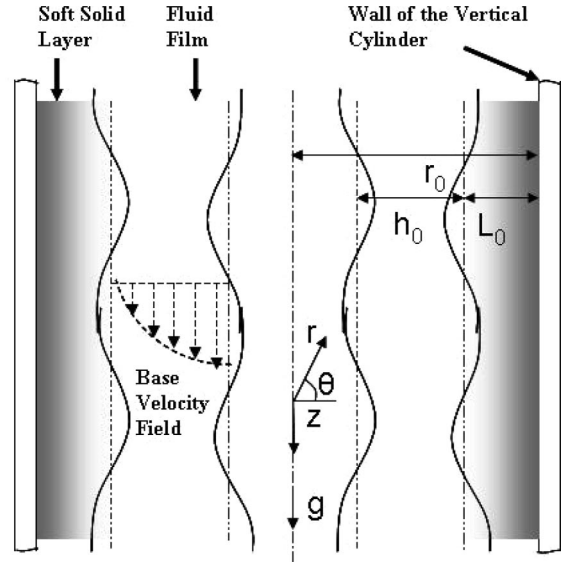

Figure 2. Schematic diagram of the configuration and coordinate system, when there is a flow inside a tube lined with a deformable solid layer. The wavy lines depict the perturbed interfaces.

$$ikRe\left[(\bar{v}_z - c)\left(d_r^2 + \frac{d_r}{r} - \frac{1}{r^2} - k^2\right) - d_r^2\bar{v}_z + \frac{d_r\bar{v}_z}{r}\right]\tilde{v}_r = d_r^4\tilde{v}_r + \frac{2}{r}\, d_r^3\tilde{v}_r - \left(\frac{3}{r^2} + 2k^2\right)\, d_r^2\tilde{v}_r + \left(\frac{3}{r^3} - \frac{2k^2}{r}\right)\, d_r\tilde{v}_r + \left(k^4 - \frac{3}{r^4} + \frac{2k^2}{r^2}\right)\tilde{v}_r \quad (23)$$

The linearized governing equations for neo-Hookean solid are

$$\frac{d\tilde{u}_r}{dR} + \frac{\tilde{u}_r}{R} + ik\tilde{u}_z - (d_R\bar{u}_z)ik\tilde{u}_r = 0 \quad (24)$$

$$-ik\tilde{p}_s + \frac{1}{\Gamma}\left(-k^2\tilde{u}_z + \frac{d^2\tilde{u}_z}{dR^2} + \frac{1}{R}\frac{d\tilde{u}_z}{dR}\right) = -k^2c^2Re\tilde{u}_z \quad (25)$$

$$(d_R\bar{u}_z)ik\tilde{p}_s - \frac{\partial\tilde{p}_s}{\partial R} + \frac{1}{\Gamma}\left(-k^2\tilde{u}_r + \frac{\partial^2\tilde{u}_r}{\partial R^2} + \frac{1}{R}\frac{\partial\tilde{u}_r}{\partial R} - \frac{\tilde{u}_r}{R^2}\right) = -k^2c^2Re\tilde{u}_r \quad (26)$$

These equations can be condensed in a single fourth-order, Orr−Sommerfeld like equation for $\tilde{v}_z$:

$$d_R^4\tilde{u}_r + \left(\frac{2k}{i}B_1 + \frac{2}{R}\right)\, d_R^3\tilde{u}_r + \left(\frac{3k}{i}B_2 + \frac{3k}{iR}B_1 - 2k^2 - k^2B_12 + \frac{\xi}{\Gamma} - \frac{3}{R^2}\right)\, d_R^2\tilde{u}_r + \left(\frac{3k}{i}B_3 + \frac{2k}{iR}B_2 - \frac{2k^3}{i}B_1 - \frac{2k^2}{R} - \frac{k^2}{R}B_12 - 2k^2B_1B_2\right)\, d_R\tilde{u}_r + \left(\frac{\xi}{\Gamma R} - \frac{2ik\xi}{\Gamma i}B_1 + \frac{3}{R^3} - \frac{2k}{iR^2}B_1\right)\, d_R\tilde{u}_r + \left(\frac{k}{i}B_4 + \frac{k}{iR}B_3 + \left(ik^3 + \frac{ik}{R^2} - \frac{\xi ik}{\Gamma}\right)B_2 - \frac{k^3}{iR}B_1 + k^4 - \frac{k^2}{R}B_1B_2 - k^2B_1B_3\right)\bar{u}_r - \left(k^4B_12 - \frac{\xi ik}{\Gamma R}B_1 - \frac{ik}{R^3}B_1 - \frac{k^2\xi}{\Gamma} - \frac{k^2\xi}{\Gamma}B_12 + \frac{2k^2}{R^2} - \frac{3}{R^4} - \frac{\xi}{R^2\Gamma}\right)\tilde{u}_r = 0 \quad (27)$$

where $B_1 = d_R\bar{v}_z$, $B_2 = d_R{}^2\bar{v}_z$, $B_3 = d_R\bar{v}_z$, $B_4 = d_R{}^4\bar{v}_z$, and $\xi = k^2c^2Re\Gamma^2$.

In both the above sets of governing equations, the first equation represents the mass conservation equation and the next two equations represents the z and r momentum balances, respectively. The interfacial conditions at gas−liquid and liquid−solid interface are linearized by Taylor-expanding the conditions about their respective mean interface positions. Hence, the linearized kinematic and boundary conditions at unperturbed free surface ($r = S \pm L \pm 1$) are

$$ik[\bar{v}_z - c]\tilde{h} = \tilde{v}_r \quad (28)$$

$$(d_r^2\bar{v}_z)\tilde{h} + \left(\frac{\partial\tilde{v}_z}{\partial r} + ik\tilde{v}_r\right) = 0 \quad (29)$$

$$-\tilde{p} + 2\frac{\partial\tilde{v}_r}{\partial r} \pm k^2\Sigma_f\tilde{h} = \frac{\pm\Sigma_f\tilde{h}}{r^2} \quad (30)$$

The sign "±" on the surface tension term indicates the two different cases of interest: flow outside and inside the cylinder. The sign is different for these two cases because of the direction of the normal unit vector n at the interface. For the outside-flow case, n points away from the center of the tube, while for the inside-flow case, n points toward the center. Next, the linearized boundary conditions at liquid−solid interface ($r = S \pm L$) are

$$\tilde{v}_r = -ikc\tilde{u}_r \quad (31)$$

$$\tilde{v}_z + (d_rv_z)_{r=S\pm L}\tilde{v}_r = -ikc\tilde{v}_z \quad (32)$$

$$(d_R\bar{u}_z)^2ik\tilde{u}_r - (d_R\bar{u}_z)\frac{\partial\tilde{u}_r}{\partial R} - ik\tilde{u}_r - \frac{\partial\tilde{u}_z}{\partial R} = -\Gamma\left(\frac{\partial\tilde{v}_z}{\partial r} + ik\tilde{v}_r\right) \quad (33)$$

$$-\tilde{p} + 2\frac{\partial\tilde{v}_r}{\partial r} + \tilde{p}_s - \frac{2}{\Gamma}\frac{\partial\tilde{u}_r}{\partial R} \pm \frac{\Sigma_i\tilde{u}_r}{(S\pm L)^2} = \pm k^2\Sigma_i\tilde{u}_r \quad (34)$$

In the boundary conditions at a liquid−solid interface, the first two equations are the conditions for continuity of velocities and the next two represent the balance of tangential and normal forces, respectively. Finally, the boundary conditions at rigid surface ($r = S$) are $r = 0$. This completes the description of equations that govern the stability of the system and the resulting set of equations can be solved for complex wavespeed c as a function of the parameters Re, k, S, L, Γ, Σ_f, and Σ_i.

3. Low-Wavenumber Analysis

In this section, we employ a low-wavenumber (or long-wave) asymptotic analysis to determine the effect of the solid deformability on the free-surface wavespeed for flow inside or outside a deformable cylindrical surface. In this problem, the complex wave speed is a function of Re, k, S, L, Γ, Σ_f, and Σ_i. However, in the limit $k \ll 1$, the complex wave speed becomes the function of Re, S, L, Γ, and Σ_f the interfacial tension parameter Σ_i does not appear in the low-wavenumber result. Subsequent calculations show that the analytical expression for $c^{(1)}$ becomes very complicated when the remaining parameters Re, S, L, Γ, and Σ_f are left unspecified. However, when the numerical values of S and L are specified, it is possible to obtain an analytical expression for $c^{(1)}$ with the other parameters left unspecified. We will first briefly outline the steps involved in the calculation of $c^{(0)}$ and $c^{(1)}$ and then discuss representative results for the outside flow. This will be followed by a brief discussion of results for flow inside the tube.

3.1. Analysis for Flow Outside the Cylinder. In the limit of very low wavenumber ($k \ll 1$), we can expand the complex wave speed corresponding to the free-surface mode in an asymptotic series in k:[9−11]

$$c = c^{(0)} + kc^{(1)} + \cdots \quad (35)$$

If we set $\tilde{v}_r \sim O(1)$, then the continuity eq 20 implies $\tilde{v}_z \sim O(k^{-1})$ and the z-momentum eq 21 implies $\tilde{p} \sim O(k^{-2})$. Therefore, the velocities and pressure in the fluid are expanded as

$$\tilde{v}_r = \tilde{v}_r^{(0)} + k\tilde{v}_r^{(1)} + \cdots \quad (36)$$

$$\tilde{u}_z = k^{-1}\tilde{v}_z^{(0)} + \tilde{v}_z^{(1)} + \cdots \quad (37)$$

$$\tilde{p} = k^{-2}\tilde{p}^{(0)} + k^{-1}\tilde{p}^{(1)} + \cdots \quad (38)$$

Similarly, the displacement field and the pressure in the solid layer are expanded as:

$$\tilde{u}_r = \tilde{u}_r^{(0)} + k\tilde{u}_r^{(1)} + \cdots \quad (39)$$

$$\tilde{u}_z = k^{-1}\tilde{u}_z^{(0)} + \tilde{u}_z^{(1)} + \cdots \quad (40)$$

$$\tilde{p}_s = k^{-2}\tilde{p}_s(0) + k^{-1}\tilde{p}_s(1) + \cdots \quad (41)$$

The Fourier coefficient of the free-surface height fluctuation \tilde h is also expanded in an asymptotic series, and $h^- \sim O(k^{-1})$ as can be inferred from eq 28. We therefore have

$$\tilde{h} = k^{-1}\tilde{h}^{(0)} + \tilde{h}^{(1)} + \cdots \tag{42}$$

Upon substituting the asymptotic expansions 35–23 in the governing stability equations for the liquid layer eqs 20–23, we obtain the following differential equations that determine the leading order and first correction to the fluid velocity field:

$$\mathrm{d}_r^4\tilde{v}_r^{(0)} + \frac{2}{r}\,\mathrm{d}_r^3\tilde{v}_r^{(0)} - \frac{3}{r^2}\mathrm{d}_r^2\tilde{v}_r^{(0)} + \frac{3}{r^3}\,\mathrm{d}_r\tilde{v}_r^{(0)} - \frac{3}{r^4}\tilde{v}_r^{(0)} = 0 \tag{43}$$

$$\mathrm{d}_r^4\tilde{v}_r^{(1)} + \frac{2}{r}\,\mathrm{d}_r^3\tilde{v}_r^{(1)} - \frac{3}{r^2}\,\mathrm{d}_r^2\tilde{v}_r^{(1)} + \frac{3}{r^3}\,\mathrm{d}_r\tilde{v}_r^{(1)} - \frac{3}{r^4}\tilde{v}_r^{(1)} = iRe\left[\left(\overline{v}_z - c^{(0)}\right)\left(\mathrm{d}_r^2 + \frac{\mathrm{d}_r}{r} - \frac{1}{r^2}\right) - \mathrm{d}_r^2\overline{v}_z + \frac{\mathrm{d}_r\overline{v}_z}{r}\right]\tilde{v}_r^{(0)} \tag{44}$$

Subsequent analysis shows that the leading-order displacement field is sufficient in the present low-k analysis, and it is governed by the following differential equation from eq 27:

$$\mathrm{d}_R^4\tilde{u}_r^{(0)} + \frac{2}{R}\,\mathrm{d}_R^3\tilde{u}_r^{(0)} - \frac{3}{R^2}\mathrm{d}_R^2\tilde{u}_r^{(0)} + \frac{3}{R^3}\,\mathrm{d}_R\tilde{u}_r^{(0)} - \frac{3}{R^4}\tilde{u}_r^{(0)} = 0 \tag{45}$$

We solve the leading-order problem and then the first correction as follows.

3.1.1. Leading Order. The governing equation for $\tilde{v}_r^{(0)}$ in the liquid layer is eq 43, and the equation for $\tilde{u}_r^{(0)}$ in the solid layer is eq 45. The boundary and interface conditions for the leading-order problem are obtained by substituting the asymptotic expansions in eqs 28–34. This results in the following conditions at $r = S + L + 1$:

$$\mathrm{d}_r\tilde{v}_z^{(0)} + (\mathrm{d}_r^2\overline{v}_z)\tilde{h}^{(0)} = 0 \tag{46}$$

$$-\tilde{p}^{(0)} = 0 \tag{47}$$

The leading-order conditions at the fluid-solid interface $r = S + L$ are given by

$$\tilde{v}_r^{(0)} = 0 \tag{48}$$

$$\tilde{v}_z^{(0)} = 0 \tag{49}$$

$$\mathrm{d}_r\tilde{v}_z^{(0)} = \frac{1}{\Gamma}\,\mathrm{d}_R\tilde{u}_z^{(0)} \tag{50}$$

$$\tilde{p}^{(0)} = \tilde{p}_s(0) \tag{51}$$

The boundary conditions at $r = S$ are simply

$$\tilde{u}_r^{(0)} = 0, \quad \tilde{u}_z^{(0)} = 0 \tag{52}$$

An important consequence of the low- k expansion of the interface conditions (eqs 31 and 32) is that, to leading-order, the fluid velocities $\tilde{v}_r^{(0)}$ and $\tilde{v}_z^{(0)}$ satisfy the no-slip conditions at $r = S + L$ as in a rigid boundary (eqs 48 and 49). This is because the right side of eqs 31 and 32 are $O(k)$ smaller than fluid velocities on the left side. This implies that the solid-layer deformability does not influence the leading-order fluid velocity field, and so the leading order wave speed in the present problem must be identical to that of Solorio and Sen's[11] analysis. However, the leading-order velocity field in the liquid layer exerts a shear stress on the solid layer via the tangential stress condition (eq 50), and this causes a deformation in the solid layer at leading order. We now present the solution to the leading-order velocity and displacement fields and the leading-order wave speed.

The general solution to differential eq 43 is simply

$$\tilde{v}_r^{(0)} = \frac{A_1}{r} + A_2 r + A_3 r\,\log\,r + A_4 r^3 \tag{53}$$

Since the stability problem is linear and homogeneous, the eigenfunction $\tilde{v}_r$ is determined only up to a multiplicative constant, and without loss of generality, we set $A_1 = 1$. The choice of this constant has no bearing on the determination of the eigenvalue. Since the expressions for $\tilde{v}_r^{(0)}$, $\tilde{v}_z^{(0)}$, and $\tilde{p}^{(0)}$ become very complicated functions of S and L, we specify these parameters here as $S = 1$ and $L = 1$. Hereafter, we will present the calculations based on these numerically specified values. After satisfying the leading-order boundary conditions 47–49, we obtain the solution to the dynamical variables in the liquid layer as

$$\tilde{v}_r^{(0)} = \frac{1}{r} + \frac{2r\,\log\,r - r\{1 + 2\,\log(2)\}}{4} \tag{54}$$

$$\tilde{v}_z^{(0)} = i\,\log\left(\frac{r}{2}\right) \tag{55}$$

$$\tilde{p}^{(0)} = 0 \qquad \text{for } S = 1, L = 1 \tag{56}$$

Upon using the leading tangential stress condition at $r = S + L + 1$ (eq 46), we obtain $\tilde{h}^{(0)} = 0.19153i$, and using the linearized kinematic condition, we obtain, to leading order

$$c^{(0)} = 2 \tag{57}$$

which is purely real and is identical to the result of Solorio and Sen[11] for a rigid cylinder. Physically, this implies that the flow is neutrally stable to leading order, and therefore, the first correction must be calculated in order to determine its stability. For subsequent analysis, we require the leading order deformation field in the solid layer, and this is obtained by solving the differential eq 45:

$$\tilde{u}_r^{(0)} = \frac{B_1}{r} + B_2 r + B_3 r\,\log\,r + B_4 r^3 \tag{58}$$

The constants are determined by the boundary conditions (eqs 50–52) to give

$$\tilde{u}_r^{(0)} = \frac{\Gamma}{4R}[1 - R^2 + 2R^2\,\log\,R] \tag{59}$$

$$\tilde{u}_z^{(0)} = i\Gamma\,\log R \tag{60}$$

$$\tilde{p}_s(0) = 0 \tag{61}$$

With these solutions, we now proceed to calculate the first correction to the wave speed $c^{(1)}$.

3.1.2. First Correction. The solution to the inhomogeneous differential eq 44 governing $\tilde{v}_r^{(1)}$ can be determined to be

$$v_r^{(1)} = \frac{C_1}{r} + C_2 r + C_3 r\,\log r + C_4 r^3 - \frac{i\tau Re}{441.29}\Big[432 - 790\tau^2 + \tau^4 + 538.88\tau^2\,\log\,\tau + 864(\log\,\tau)^2 - 54\tau^2\log\left[\frac{\tau}{2}\right](-5 + 4\,\log\,\tau)\Big]$$

The constant C_1 can be set to zero without loss of generality since we have already fixed the constant multiplying the term $1/r$ to be 1 at leading order. The other constants are obtained from eqs 28–31) as follows. At $r = S + L + 1$, the first correction to the tangential and normal stress conditions become

$$\mathrm{d}_r \bar{v}_z^{(1)} + (\mathrm{d}_r^2 u_z)\tilde{h}^{(1)} = 0 \tag{62}$$

$$-\tilde{p}^{(1)} = \frac{\Sigma_f \tilde{h}^{(1)}}{r^2} \tag{63}$$

At $r = S + L$, the first correction to the velocity continuity conditions become

$$\tilde{v}_r^{(1)} = -ic^{(0)}\tilde{u}_r^{(0)} \tag{64}$$

$$\tilde{v}_z^{(1)} = -(\mathrm{d}_r v_z)\tilde{u}_r^{(0)} - ic^{(0)}\tilde{u}_z^{(0)} \tag{65}$$

Note here that, in contrast to a rigid inclined surface, the deformation in the solid layer appears in the normal and tangential velocity conditions: the leading order deformation field in the solid layer affects the first correction to the fluid velocity field. Using the conditions 63–65, the constants C_2, C_3, and C_4 are determined to give

$$\begin{aligned}\tilde{v}_r^{(1)} = &-0.00226iRer^5 + 0.489iRer^3 \log r^2 + 2.807iRer^3 - \\ &0.001i\Sigma_f r^3 - 2.163iRer^3 \log r - 1.958iRer \log r^2 - \\ &0.278i\Gamma r - 2.736iRer - 0.002i\Sigma_f r - 0.0579i\Gamma r \log r - \\ &3.547iRer \log r + 0.010i\Sigma_f r \log r\end{aligned} \tag{66}$$

Using this result for $\tilde{v}_z^{(1)}$, the first correction to the height fluctuation $\tilde{h}^{(1)}$ can be calculated from eq 62 to give

$$\tilde{h}^{(1)} = 0.022\Gamma + 0.075Re + 0.01426\Sigma_f \tag{67}$$

The first correction to the wave speed $c^{(1)}$ is then obtained from the first correction to the kinematic condition (28):

$$i[\bar{v}_z(r = S + L + 1) - c^{(0)}]\tilde{h}^{(1)} - ic^{(1)}\tilde{h}^{(0)} = \tilde{v}_r^{(1)}(r = S + L + 1) \tag{68}$$

In the above equation, all the quantities except $c^{(1)}$ are now calculated, so $c^{(1)}$ can be obtained as

$$c^{(1)} = i[-5.235\Gamma + 0.611Re + 0.0379\Sigma_f] \tag{69}$$

which is a purely imaginary quantity and hence dictates the stability of the system. Importantly, the term multiplying the solid deformability parameter Γ is negative, indicating that the deformable solid has a stabilizing effect on the free-surface instability.

It is useful at this point to discuss the physical reason behind the stabilizing effect of the solid deformability. A detailed explanation of the mechanism underlying the free-surface instability of planar film flow is given by Kelly et al.[20] and Smith.[21] They carried out an energy balance analysis and identified the dominant energy production term to be the work done by the perturbation shear stress at the free surface. Here, we demonstrate that the perturbation shear stress at the free surface is qualitatively altered by the deformability of the solid layer. To this end, it is useful to consider the first correction to the kinematic condition, eq 62. This equation relates the first correction to the height fluctuation $\tilde{h}^{(1)}$ to the first correction to the shear stress in the liquid at the free surface. Therefore, $c^{(1)}$ calculated using eq 68 is also dependent on $\mathrm{d}_r \tilde{v}_z^{(1)}|_{r = S+L+1}$. As pointed out in the preceding discussion, the destabilizing term due to fluid inertia (proportional to *Re*) appears only at the first correction to the fluid velocity field, which arises from the first correction to the tangential stresses at the free surface. In addition to this inertial contribution, and in contrast to a rigid surface, the deformation in the soft solid layer creates a perturbation flow (proportional to Γ), which also appears at $O(k)$. This contribution will alter the first correction to the tangential stress at the free surface. If the perturbation flow at $O(k)$ due to the solid deformation opposes the flow due to fluid inertia, then one would expect this to result in stabilization the free-surface instability. Our asymptotic calculations indeed show this to be the case, thus resulting in the stabilizing nature of solid layer deformability on the free-surface instability.

Table 1. Effect of the Radius of Curvature of the Cylinder (*S*) on $c^{(0)}$ and $c^{(1)}$: Flow Outside the Rigid Cylinder ($L = 0$ or $\Gamma = 0$)

S	$c^{(0)}$	$c^{(1)}$
1	2	$(0.6759Re + 0.088761\Sigma_f)i$
5	2	$(0.567Re + 0.009304\Sigma_f)i$
10	2	$(0.551Re + 0.002758\Sigma_f)i$
50	2	$(0.537Re + 0.000128\Sigma_f)i$
100	2	$(0.535Re + 0.000032\Sigma_f)i$

We next discuss some representative results for the case of flow outside the cylinder, when the wall is rigid, after which we examine the role of wall deformability.

3.1.3. Results for a Rigid Cylinder. For a rigid cylinder (i.e., $L = 0$ or $\Gamma \to 0$), we have to specify the value of S to get the analytical expressions for $c^{(0)}$ and $c^{(1)}$. For example, when $S = 1$, the results for $c^{(0)}$ and $c^{(1)}$ from our analysis are

$$c^{(0)} = 2 \tag{70}$$

$$c^{(1)} = i[0.6759Re + 0.0887611\Sigma_f] \tag{71}$$

At leading order, the wave speed is a real quantity and is always given by 2; i.e., the dimensional wave speed is twice the free-surface laminar velocity. The first correction to the complex wave speed is purely imaginary and depends on these independent parameters: *Re*, *S*, and Σ_f. The first correction $c^{(1)}$ has two contributions: the term proportional to *Re* is destabilizing and has been termed by Lin and Liu[9] as an inertial instability. The second contribution is again destabilizing, and this is the term proportional to surface tension parameter Σ_f. This instability is caused by the curvature of the free surface of the annular film, which is destabilized by surface tension or capillary forces. This is akin to the classical Rayleigh (or "capillary") instability of a liquid jet.[4] This contribution is absent for a planar liquid film. As we can observe from the above result, the flow is unstable even at zero inertia (i.e., $Re = 0$) due to the capillary forces at the free surface. Therefore, this flow can never be stable at any value of *S*, which is shown in Table 1. We can clearly see from Table 1 that as we increase the radius of curvature (*S*) of the cylinder, the contribution from the *Re* term decreases slightly. The contribution from the Σ_f term decreases rapidly and approaches zero asymptotically at a very high radius of curvature of the cylinder. This is because, for large *S*, one eventually approaches the asymptotic limit of a film falling down a flat plate. It is further useful to note that the value of $c^{(0)}$ and $c^{(1)}$ for $S = 100$ (the limit of a film falling down a flat plate) is identical to the result obtained by Yih,[7] except for the different nondimensionalization scheme used here. Thus, for rigid cylinders, the flow configuration can never be stabilized by tuning all the parameters present in the system. We next consider the effect of a soft deformable solid coating over the rigid cylinder.

3.1.4. Effect of Solid Deformability. We now present results showing the effect of the deformable solid layer on the numerical value and sign of $c^{(1)}$, which determines the stability characteristics of the flow configuration. Here again we have to specify the numerical value of *S* and *L* to get the analytical results. We choose different sets of values of *S* and *L* and show the effect of these two parameters on $c^{(1)}$. For example, when $S = 1$, $L = 1$, the results for $c^{(0)}$ and $c^{(1)}$ from our analysis are

$$c^{(0)} = 2 \tag{72}$$

$$c^{(1)} = i[-5.235\Gamma + 0.611Re + 0.0379\Sigma_f] \quad (73)$$

The leading order complex wave speed, $c^{(0)}$, still remains real, and is identical to the result for a rigid cylinder. At leading order, the solid deformability does not influence the leading-order fluid velocity field, and so the leading-order wave speed might be expected to be identical to the rigid cylinder. The stability of the system is determined by the first correction to the complex wave speed, which is purely imaginary, and depends on the following parameters: Re, S, L, Γ, and Σ_f. There are three contributions to $c^{(1)}$ now: apart from the destabilizing contributions proportional to Re and Σ_f, there is one stabilizing term due to solid deformability, proportional to Γ. The solid elasticity parameter $\Gamma = \mu V/(Gh_0)$ tends to zero in the limit of rigid solid layer (i.e., the shear modulus G of the solid layer becomes large compared to the viscous shear stresses in the fluid). However, as the shear modulus G decreases, Γ increases, thus making the solid layer more deformable. The numerical coefficients multiplying the three terms in $c^{(1)}$ depend on the values of S and L. We have already seen the effect of S on terms proportional to Re and Σ_f terms while discussing the rigid cylinder result. The effect of increasing the radius of curvature S, for a fixed L, on the term proportional to Γ is illustrated in Table 2.

As seen from these results, the contribution from the term proportional to Γ decreases and approaches to 4 asymptotically at a very high radius of curvature of the cylinder. In the limit of very high radius of curvature ($S \gg 1$), the present results reduce to the case of planar liquid film flow past a deformable solid layer analyzed in Shankar and Sahu.[13] The results presented in Table 2 demonstrate that, for any particular value of S, it is possible to tune the other parameters to have stable or unstable flow configuration.

In order to examine the effect of solid deformability on the capillary instability (due to surface tension and curvature), it is necessary to keep the curvature of the free surface in the base state to be a constant. This is achieved by keeping $S + L$ constant and by varying L (and therefore S), as illustrated in Table 3. As L is increased from zero (i.e., no deformable solid), with $S + L$ kept constant, the solid deformability becomes more stabilizing, while while the inertial and capillary contributions remain constant for a fixed $S + L$. The inertial and capillary contributions are thus only a function of the curvature of the base state, while the deformable solid contribution becomes more stabilizing as L increases.

Table 2. Effect of the Radius of Curvature of the Cylinder (S) on $c^{(0)}$ and $c^{(1)}$: Flow Outside the Cylinder Coated with Soft Solid of Thickness $L = 1$

S	$c^{(0)}$	$c^{(1)}$
1	2	$(-5.235\Gamma + 0.6114Re + 0.037895\Sigma_f)i$
5	2	$(-4.269\Gamma + 0.561Re + 0.0068\Sigma_f)i$
10	2	$(-4.1344\Gamma + 0.549Re + 0.002317\Sigma_f)i$
50	2	$(-4.026\Gamma + 0.537Re + 0.000123\Sigma_f)i$
100	2	$(-4.0131\Gamma + 0.535Re + 0.000032\Sigma_f)i$

Table 3. Effect of Solid Deformability at Constant Curvature of the Free Surface ($S+L = 10$): Flow Outside the Cylinder Coated with Soft Solid of Thickness L^a

S	L	$c^{(1)}$
2	8	$(-50.641\Gamma + 0.5503Re + 0.00275\Sigma_f)i$
4	6	$(-30.7575\Gamma + 0.5503Re + 0.00275\Sigma_f)i$
6	4	$(-18.274\Gamma + 0.5503Re + 0.00275\Sigma_f)i$
8	2	$(-8.510\Gamma + 0.5503Re + 0.00275\Sigma_f)i$
10	0	$(0.5503Re + 0.00275\Sigma_f)i$

[a] $c^{(0)}$ remains constant at 2.

Table 4. Effect of the Radius of Curvature of the Cylinder (S) on $c^{(0)}$ and $c^{(1)}$: Flow Inside a Rigid Cylinder ($L = 0$ or $\Gamma = 0$)

S	$c^{(0)}$	$c^{(1)}$
2	2	$(0.4321Re + 0.360787\Sigma_f)i$
5	2	$(0.4964Re + 0.020995\Sigma_f)i$
10	2	$(0.5154Re + 0.004122\Sigma_f)i$
50	2	$(0.5298\mathrm{Re} + 0.000138\Sigma_f)i$
100	2	$(0.5347Re + 0.000034\Sigma_f)i$

Table 5. Effect of solid deformability at constant curvature of the free-surface ($S - L - 1 = 1$). Flow inside the cylinder coated with soft solid of thickness L^a.

S	L	$c^{(1)}$
10	8	$i(-43.1685\Gamma + 0.432108Re + 0.360787\Sigma_f)$
6	4	$i(-16.8817\Gamma + 0.432108Re + 0.360787\Sigma_f)$
5	3	$i(-11.9446\Gamma + 0.432108Re + 0.360787\Sigma_f)$
4	2	$i(-7.57723\Gamma + 0.432108Re + 0.360787\Sigma_f)$

[a] $c^{(0)}$ remains constant at 2.

3.2. Results for Flow Inside the Cylinder. Here we merely show the results for flow inside the cylinder and eschew the details of the calculation as they are similar to the one outlined above. For the rigid cylinder, it is necessary to specify the value of S to get the analytical expressions for $c^{(0)}$ and $c^{(1)}$. In this case, the value of S should always be greater than 1 because of the boundedness of the problem. For example, when $S = 2$, the results for $c^{(0)}$ and $c^{(1)}$ from our analysis are

$$c^{(0)} = 2 \quad (74)$$

$$c^{(1)} = i[0.432108Re + 0.360787\Sigma_f] \quad (75)$$

As we can observe from the above result, here also the flow is unstable even at zero inertia ($Re = 0$) due to the capillary forces at the free surface. Therefore. this flow can never be stable at any value of S, which is shown in Table 4. We can clearly see from the Table 4 that as we increase the radius of curvature (S) of the cylinder, the contribution from the Re term increases slightly and hence contributes a destabilizing effect to $c^{(1)}$, which is opposite to the behavior seen for the outside case. However, in the limit $S \gg 1$, the coefficient multiplying the Re term in Table 4 for flow inside the cylinder approaches the value for flow outside the cylinder given in Table 1. But the contribution from the Σ_f term decreases rapidly and approaches to zero asymptotically at a very high radius of curvature of the cylinder similar to the outside case. Thus, this flow configuration can never be stabilized by tuning the parameters present in the system. We next examine the effect of a soft solid coating on the inner side of the rigid cylinder. While specifying the value of S and L to get the analytical results, the geometry of the problem imposes the constraint $S - L - 1 > 0$. As per this criterion, we choose different sets of values of S and L, such that $S - L - 1$ is kept constant and analyze the effect of these two parameters on $c^{(0)}$ and $c^{(1)}$. Table 5 shows representative results for flow inside a cylinder lined with a deformable wall. As in the case of outside flow, the (destabilizing) contributions due to inertia and capillary forces remain constant for fixed value of $S - L - 1$, while the (stabilizing) contribution due to the deformable solid layer increases with increase in L. Thus, for any particular value of S we can tune the other parameters to have stable or unstable flow configuration.

The above asymptotic results for both the geometries are only applicable in the low-wavenumber limit. In practical applications, the wavenumber of disturbances can be arbitrary. In order to determine whether the predicted stabilization extends to perturbations with finite and high wavenumber, it is necessary to solve the governing stability equations, boundary and interface

conditions numerically. In addition, at finite wavenumber, the interfacial mode corresponding to the solid−fluid interface can also become unstable when Γ is increased beyond a critical value. In the next section, we use the numerical solution to determine regions in the Γ − k plane where both the modes (liquid−solid interface and free surface) are stable.

4. Results at Arbitrary Wavenumbers

4.1. Numerical Method. We first briefly describe the numerical method used to obtain the eigenvalue for arbitrary k. There are two fourth-order ordinary differential equations (ODEs) in the fluid and in the solid layer. We use a fourth-order Runge−Kutta integrator with adaptive step size control to obtain numerical representations of the linearly independent solutions to the fourth-order ODEs. We recast the fourth-order ODE in each layer as a system of first-order differential equations[5] for the variables $[\tilde{u}_r, \mathrm{d}_R\tilde{u}_r, \mathrm{d}_R{}^2\tilde{u}_r, \mathrm{d}_R{}^3\tilde{u}_r]$. For the solid, this system of first-order equations can be integrated from $R = S$ to $R = S \pm L$ ("+" sign denotes outside flow while "−" sign denotes inside flow), provided the values of $_r$ and its first three derivatives are known at $R = S$. The solid displacement $\tilde{u}_r$ satisfies the boundary conditions $\tilde{u}_r = 0$ and $\tilde{u}_z = 0$ at $R = S$. We use two different sets of higher derivatives $\mathrm{d}_R{}^2\tilde{u}_r$ and $\mathrm{d}_R{}^3\tilde{u}_r$ at $R = S$ that are consistent with the boundary conditions at $R = S$, which will yield the two linearly independent solutions to the solid displacement:

$$\tilde{u}_r = 0, \quad \mathrm{d}_R\tilde{u}_r = 0, \quad \mathrm{d}_R^2\tilde{u}_r = 1, \quad \mathrm{d}_R^3\tilde{u}_r = 0 \tag{76}$$

$$\tilde{u}_r = 0, \quad \mathrm{d}_R\tilde{u}_r = 0, \quad \mathrm{d}_R^2\tilde{u}_r = 0, \quad \mathrm{d}_R^3\tilde{u}_r = 1 \tag{77}$$

Using these conditions at $R = S$, we use the Runge−Kutta method to integrate the ODE in solid up to $R = S \pm L$. The displacement $\tilde{u}_r$ in the solid is then obtained as linear combination of these two solutions (denoted by $\tilde{u}_r{}^{(1)}$ and $\tilde{u}_r{}^{(2)}$), and this displacement field is consistent with the boundary conditions at $R = S$:

$$\tilde{u}_r = A_1\tilde{u}_r^{(1)} + A_2\tilde{u}_r^{(2)} \tag{78}$$

where A_1 and A_2 are constants to be determined from the conditions at the interface. Corresponding to these two linearly independent solutions, we evaluate the velocity field of the fluid $\tilde{v}_r$ and its higher derivatives from the interfacial conditions at r (or R) $= S \pm L$ (eqs 31–34). Using these two sets of values for $\tilde{v}_r$ and its derivatives, we integrate the fourth-order differential equation in the fluid from $r = S \pm L$ to $r = S \pm L \pm 1$. The velocity field in the fluid is obtained as a linear combination of these two solutions. At $r = S \pm L \pm 1$, the fluid velocity field must satisfy the free-surface conditions given by (29) and (30). This is written in a matrix form, and the determinant of this matrix is set to zero to obtain the characteristic equation This is solved numerically using a Newton−Raphson iteration procedure to obtain the eigenvalue c for specified values of $Re, k, S, L, \Gamma, \Sigma_f$, and Σ_i. We specify the values of these parameters as follows: For a Newtonian fluid, we choose the value of the viscosity to be $10^{-1}-10^{-2}$ Pa·s. We choose fluid film thickness to equal $h_0 \sim 1-10$ mm. The density of liquids is ∼1000 kg/m^3, the surface and interfacial tension is $\sim O(10^{-2})$ N/m, and acceleration due to gravity is ∼10 m/s^2. After substituting all these dimensional parameters values in the nondimensional parameters, we obtain $Re \sim O(1)$, $\Gamma \sim 100/\mathrm{G}$, $H \sim O(1)$, $\Sigma_f \sim O(1)$ and $\Sigma_i \sim O(1)$. We now use the low-k asymptotic results as a starting guess for the for the numerical procedure and continue the low-k results numerically to finite values of k. The results from the numerical method were first validated by comparing it with the predictions of the asymptotic analysis.

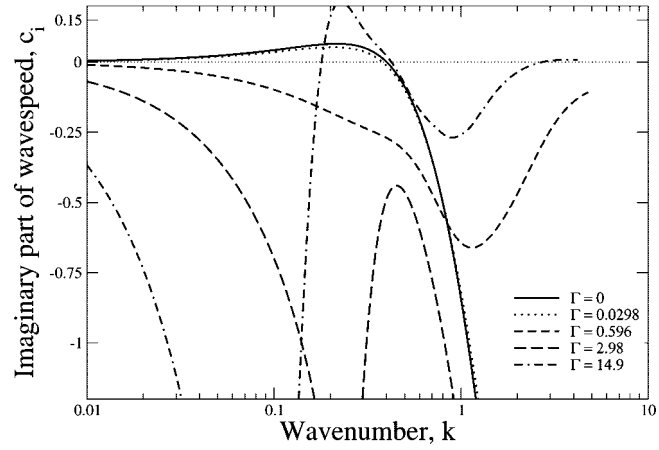

Figure 3. Effect of solid layer deformability on mode 1: c_i vs k data (continued from low k results) for $Re = 0$, $S = 1$, $L = 0.5$, $\Sigma_f = 8.385$, and $\Sigma_i = 0$.

4.2. Results for Flow Outside the Cylinder. We will demonstrate the effect of solid deformability on the stability characteristics of the flow configuration after a brief review of the results of flow down a vertical rigid cylinder carried out earlier.[11] We use the low-k asymptotic results from the preceding section as a starting guess, and use the numerical procedure outlined above to continue the low-k results to finite values of k. We shall use the term "mode 1" for the results obtained from the continuation of low-k asymptotic result, which denotes the stability characteristics of the gas−liquid interface in the long-wave limit. Figure 3 shows the variation of the imaginary part of the complex wave speed c_i as a function of the wavenumber k. The solid curve, which represents the flow down a rigid cylinder for $Re = 0$, $S = 1$, and $\Sigma_f = 8.385$, indicates that c_i is positive (mode 1 is unstable) from $k \ll 1$ to $k \sim 0.4$, and for larger values of k, the system is stable. This instability (at finite k) has been well explained by Solorio and Sen.[11] We now examine the effect of wall deformability on this instability at arbitrary wavenumbers. It must be noted that due to the deformability of the solid, we may observe one more instability caused by the solid−liquid interface. This instability was first analyzed by Kumaran et al.[22] for plane Couette flow past a linear elastic solid, and they showed that the solid−liquid interface becomes unstable at finite wavelengths when Γ increases beyond a particular value. To obtain the solution for the complex wave speed corresponding to the liquid−solid interface (at low- k), we use a $Re = 0$ analysis (similar to Kumaran et al.),[22] where an analytical solution is possible for arbitrary k to obtain a starting guess, and use the numerical procedure outlined above to continue the $Re = 0$ results. The analysis at $Re = 0$ yields two solutions to wave speed c, one corresponding the gas−liquid interfacial mode (mode 1) in the long-wave limit, and the other solution to c is identified with the liquid−solid interface. We shall use the term "mode 2" for this solution. Although mode 1 and mode 2 dictate the stability characteristics of the system at low-k, respectively, for gas−liquid and liquid−solid interfaces, at finite and high k, we find that these two modes may interchange their behavior. In the following discussion, we address the issues pertaining to the effect of solid deformability on both the modes.

We first discuss the results showing the effect of solid deformability on the stability characteristics of the mode 1. Figure 3 shows the c_i versus k curves for $Re = 0$, $S = 1$, $L =$

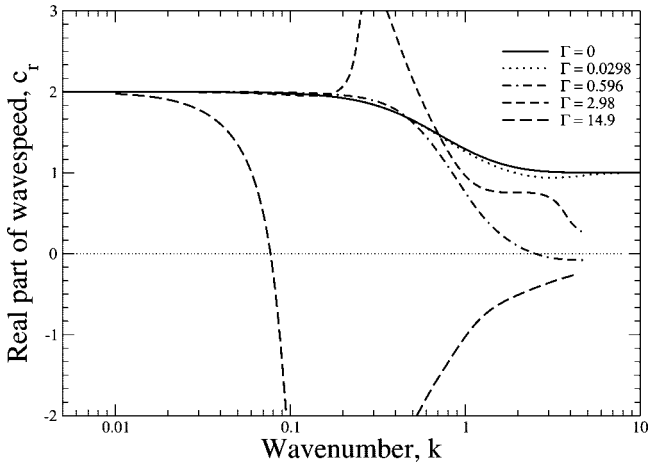

Figure 4. Demonstration of the mode switching phenomenon: c_r vs k data (continued from low k results) for $Re = 0$, $S = 1$, $L = 0.5$, $\Sigma_f = 8.385$, and $\Sigma_i = 0$.

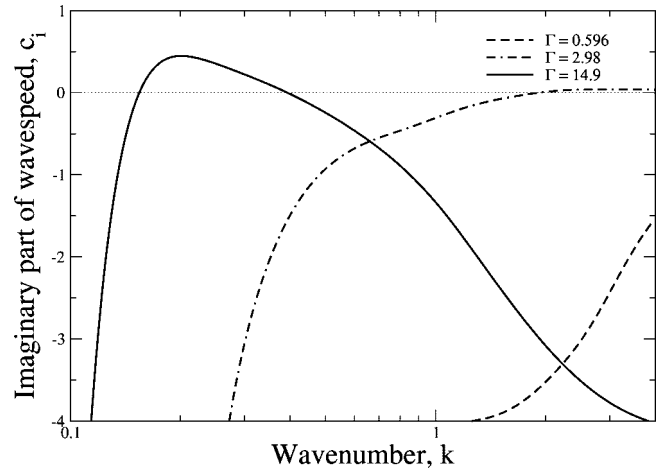

Figure 5. Effect of solid layer deformability on mode 2: c_i vs k data (continued from $Re = 0$ results) for $Re = 0$, $S = 1$, $L = 0.5$, $\Sigma_f = 8.385$, and $\Sigma_i = 0$.

0.5, $\Sigma_f = 8.385, \Sigma_i = 0$. and various values of Γ. As Γ is increased form 0 (rigid case) to 0.0298 (still sufficiently rigid), the cutoff wavenumber (for $k >$ cutoff wavenumber, mode 1 becomes stable) decreases from 0.4 to 0.38. Further increasing the value of Γ to 0.596 and 2.98, the mode 1 instability is suppressed by the solid layer at all wavenumbers. For nonzero values of Γ, the behavior of the c_r and c_i versus k curve for mode 1 is expected to be similar to the rigid case ($\Gamma = 0$) in the low- and high-k limit for the following reason. At low k, our foregoing asymptotic analysis implies that the wave speed in the presence of the deformable solid layer remains identical to the rigid case. Even at high k, because the decay length for the velocity disturbances scales as $O(k^{-1})$, perturbations at any interface are localized and so there is no effect of the deformability of solid layer on the perturbations at the gas−liquid interface. We therefore expect the real part of the wave speed (c_r) for the rigid vertical cylinder and for the vertical cylinder coated with soft solid to be nearly equal at low and high wavenumbers. This expectation is also borne out in the c_r versus k plots shown in Figure 4. For $\Gamma = 0.0298$, the values of c_r for mode 1 is almost identical to the c_r values corresponding to the rigid cylinder at high wavenumbers. This confirms that the mode 1 dictates the stability characteristics of the system for the gas−liquid interface for $\Gamma = 0.0298$ at all wavenumbers. However, when we increase the value of Γ to 0.596, 2.98, and 14.9, we observe that at high wavenumbers the value of c_r does not approach the rigid cylinder results, but instead asymptotes to some other behavior. This indicates that the characteristics of the mode 1 has "switched" to some other mode in the system. At zero Re, there are only two possible unstable modes, viz., capillary instability at the gas−liquid interface and instability caused by the liquid−solid interface. Hence, mode 1, which represents the gas−liquid interfacial mode at low k, has switched its behavior at high k and now exhibits behavior typical of the liquid−solid interface at high k. Correspondingly, when we plot the c_i versus k curve for $\Gamma = 14.9$, we observe the onset of the instability at $k \sim 0.18$ and this instability exists up to $k \sim 0.42$; there is again another instability at high wavenumbers for the same mode. This is because of mode-switching, whereby mode 1 (while exhibiting the characteristics of the gas−liquid interface at low k), exhibits an instability caused by the liquid−solid interface at finite and high k.

We next discuss the stability characteristics of the mode 2. which is obtained from the $Re = 0$ analysis, and therefore would nominally correspond a solution that corresponds to the

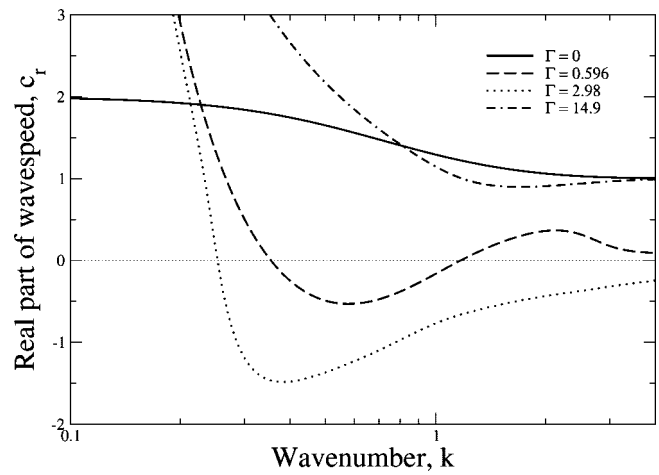

Figure 6. Demonstration of the mode switching phenomenon: c_r vs k data (continued from $Re = 0$ results) for $Re = 0$, $S = 1$, $L = 0.5$, $\Sigma_f = 8.385$, and $\Sigma_i = 0$.

liquid−solid interface. Figure 5 shows the c_i versus k plots for $\Gamma = 0.596$, 2.98, and 14.9. For $\Gamma = 0.596$, mode 2 is stable at all k while for $\Gamma = 2.98$ we observe a high-k instability caused by liquid−solid interface and due to the first normal stress difference in the neo-Hookean solid. When $\Gamma = 14.9$, we observe a finite-k instability. This instability, although continued using the liquid−solid mode from the $Re = 0$ analysis, belongs to the gas−liquid interface because of mode switching. The mode switching phenomenon for mode 2 can be seen in Figure 6 where c_r is plotted versus k and data in this figure are obtained from the continuation of $Re = 0$ result.

In this figure, the curves for $\Gamma = 0.596$, 2.98 remain mode 2 as they do not follow the c_r values of the rigid cylinder, while the $\Gamma = 14.9$ curve follows the c_r values for mode 1 of the rigid cylinder. Hence, at $\Gamma = 25$, mode switching has already occurred. Therefore, at finite k, we obtain the stability characteristics of the gas−liquid interface by the continuation of $Re = 0$ result and that of the liquid−solid interface by the continuation of low-k result corresponding to the gas−liquid interface. However, from a practical point of view, we are interested in parametric regimes where there are no unstable modes, and mode-switching plays no role to that end. The results presented thus far are for the growth rate (proportional to c_i) versus k for a fixed value of Γ.

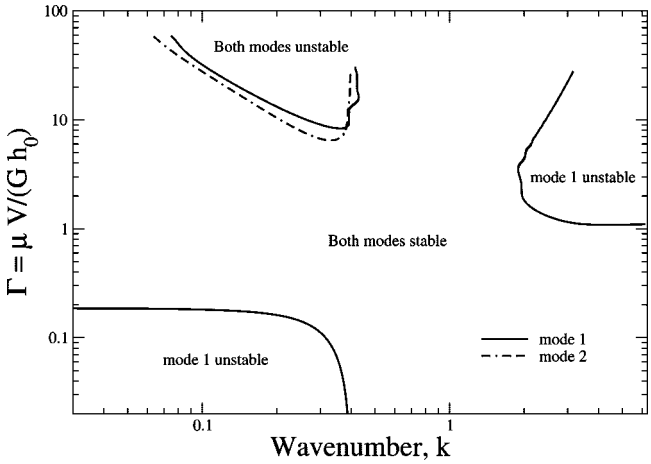

Figure 7. Neutral stability curves in Γ-k plane for flow outside the cylinder: $Re = 0$, $S = 1$, $L = 0.5$, $\Sigma_f = 8.385$, and $\Sigma_i = 0$.

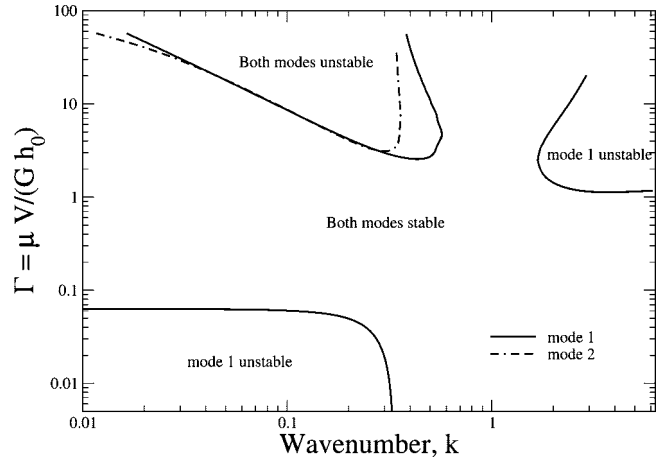

Figure 8. Neutral stability curves in Γ-k; plane for flow outside the cylinder: $Re = 0$, $S = 1$, $L = 1$, $\Sigma_f = 8.7$, and $\Sigma_i = 0$.

It is useful to present the stability results in terms of a "neutral stability diagram" in the Γ−k plane where stable and unstable regions are demarcated. Figure 7 presents the neutral stability diagram for $Re = 0$, $S = 1$, $L = 0.5$, $\Sigma_f = 8.385$, and $\Sigma_i = 0$.

Recall that $\Gamma = 0$ is the limit of a rigid cylinder, and in that limit, mode 1 (belongs to the gas−liquid interface) is unstable for $k \leq 0.4$ (also see the c_i vs k curve in Figure 3). As Γ is increased beyond the lower neutral curve, there is transition from unstable to stable perturbations of mode 1. There is large range of the parameter Γ where the mode 1 is stabilized by the solid-layer deformability. As Γ is increased further, there is another neutral curve at finite k where there is a transition from stable to unstable perturbations. This instability, as we have discussed earlier, is obtained from the continuation of $Re = 0$ results but dictates the instability caused by the gas−liquid interface (due to mode switching). We obtain another finite k instability by continuation of low k results but this, now, dictates the instability caused by the liquid−solid interface. The high wavenumber instability shown by this neutral curve is because of the first normal stress difference present in the neo-Hookean solid. It is important to emphasize that we are interested only in the window of stable region (in Γ) between the lower and upper neutral curves, from which the shear modulus value of the deformable solid can be chosen where the free-surface instability is suppressed. The effect of the thickness of the solid layer on the upper curves (at the finite k) are similar to that found in the work of Shankar and Sahu[13] and Gaurav and Shankar.[14] They had demonstrated (for the planar geometry) that the upper curves shift downward by increasing the thickness of the solid layer (i.e., destabilizing effect of L). We have also found the same behavior for the two finite k upper curves, when we increase the value of L from 0.5 to 1 and 2, which is shown in Figures 8 and 9 for $L = 1$ and 2, respectively.

In contrast, increase in the thickness of the solid layer has a stabilizing effect on the lower curve as well as the high-k instability curve; i.e., upon increasing the value of L, lower curve moves down and high-k instability curve moves up. The reason for this different behavior on the lower curve is related to the radius of curvature of the cylinder. When we increase the thickness of the solid layer, the radius of curvature of the cylinder increases. The lower curve is mainly because of the capillary instability (at $Re = 0$), which is related to the radius of curvature of the cylinder because the destabilizing capillary force is inversely proportional to the radius of curvature. Therefore, the lower curve moves down (stabilized) by increasing the thickness of the solid layer. It has also been observed

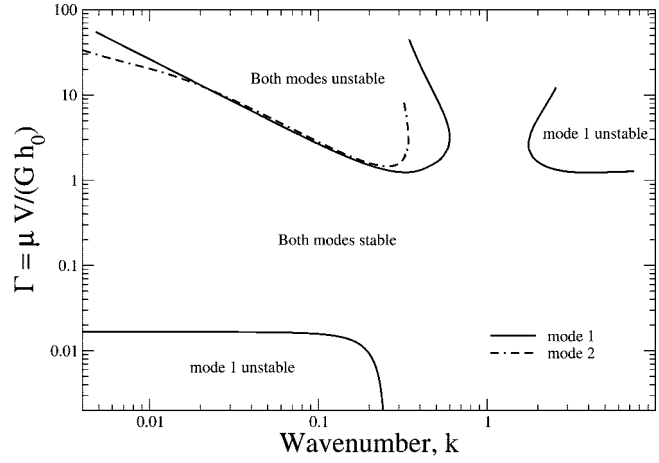

Figure 9. Neutral stability curves in Γ−k plane for flow outside the cylinder: $Re = 0$, $S = 1$, $L = 2$, $\Sigma_f = 9.07$, and $\Sigma_i = 0$.

by Solorio and Sen[11] that increasing the radius of curvature of the cylinder stabilizes the capillary instability for rigid cylinder. The high-k instability curve moves up because the destabilizing normal stress difference decreases upon increase in the solid thickness. We next increase the radius of curvature of the cylinder by increasing S and examine the effect on the neutral stability curves. We now choose the parameters $Re = 0$, $S = 2$, $L = 0.5$, $\Sigma_f = 8.914$, and $\Sigma_i = 0$ and present the neutral curves in Figure 10.

The effect of increasing S on all the neutral curves is stabilizing; i.e., lower neutral curve shifts down and all the upper neutral curves shift upward. When S is further increased to 10, we do not observe the finite k upper neutral curves as can be seen in Figure 11.

However, at the same value of $S = 10$, when we increase the solid-layer thickness from 0.5 to 1, the finite k upper neutral curves appear thus further corroborating the destabilizing effect of increasing solid-layer thickness (see Figure 12).

We have thus far presented the results for zero Re. Next, we study the effect of Reynolds number on neutral stability curves. We choose the parameters $Re = 0.298$, $S = 1$, $L = 0.5$, $\Sigma_f = 8.385$, $\Sigma_i = 0$ and show the neutral stability diagram in Figure 13.

If we compare $Re = 0$ and $Re = 0.298$ results, we find that the Reynolds number has a destabilizing effect on both the modes: the lower neutral curve moves up and all the upper neutral curves move down. Further increasing Re from 0.298

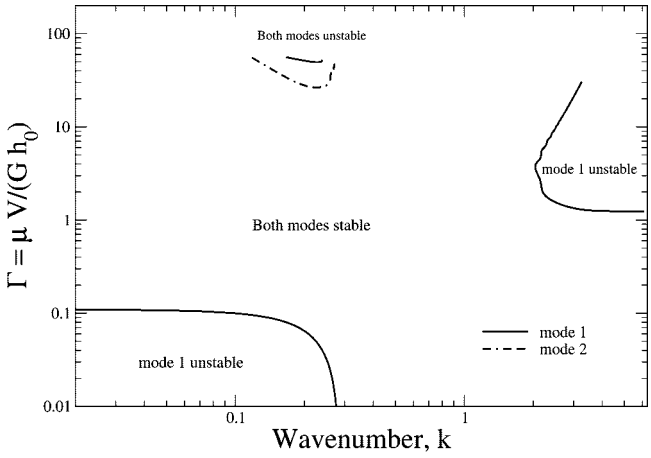

Figure 10. Neutral stability curves in $\Gamma-k$ plane for flow outside the cylinder: $Re = 0$, $S = 2$, $L = 0.5$, $\Sigma_f = 8.914$, and $\Sigma_i = 0$.

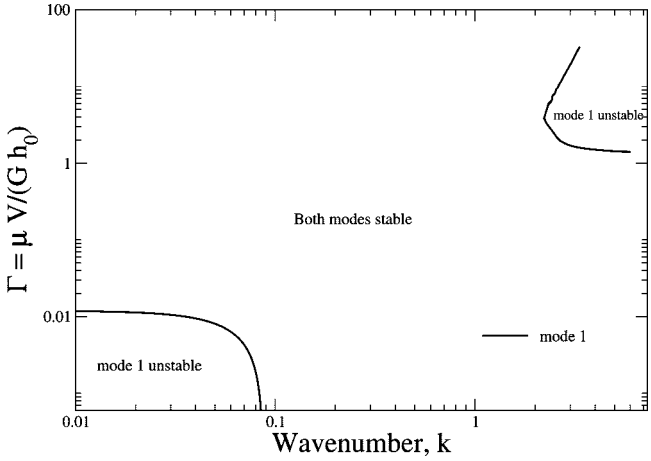

Figure 11. Neutral stability curves in $\Gamma-k$ plane for flow outside the cylinder: $Re = 0$, $S = 10$, $L = 0.5$, $\Sigma_f = 9.7$, and $\Sigma_i = 0$.

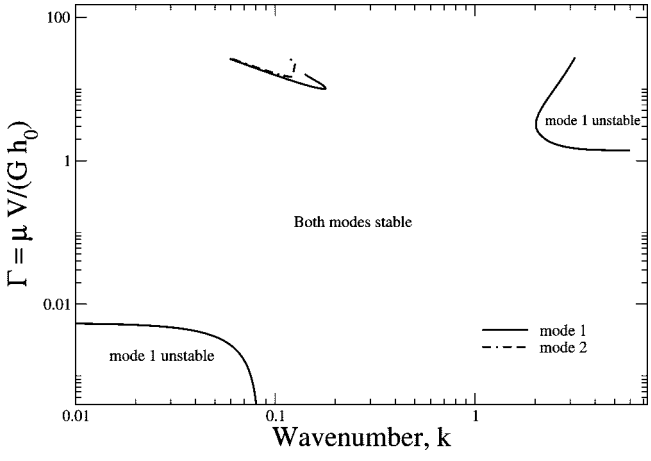

Figure 12. Neutral stability curves in $\Gamma-k$ plane for flow outside the cylinder: $Re = 0$, $S = 10$, $L = 1$, $\Sigma_f = 9.71$, and $\Sigma_i = 0$.

to 1.192, causes the merging of the finite k upper mode 1 and high-k mode 1 curves, which can be seen in Figure 14. The effect of Re is similar for other values of S and L (data not shown). Instead, for the parameters $Re = 0.055$, $S = 1$, $L = 2$, $\Sigma_f = 8.385$, and $\Sigma_i = 0$, we obtain two new modes (mode 3 and mode 4) at high Γ as can be seen in Figure 15. These modes were absent for $Re = 0$, and hence, we refer to these modes as "inertial modes" because of their presence only at finite Re.

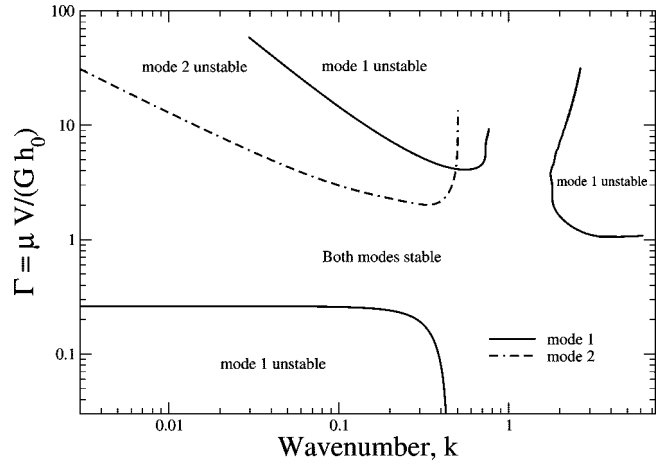

Figure 13. Neutral stability curves in Γ–k plane for flow outside the cylinder: Re = 0.298, $S = 1$, $L = 0.5$, $\Sigma_f = 8.385$, and $\Sigma_i = 0$.

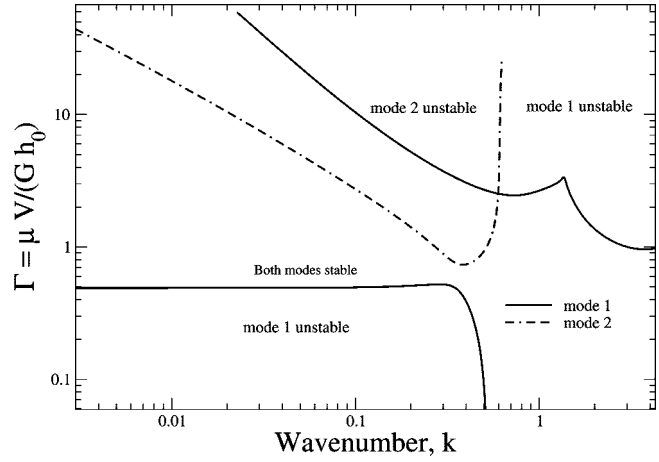

Figure 14. Neutral stability curves in $\Gamma-k$ plane for flow outside the cylinder: $Re = 1.192$, $S = 1$, $L = 0.5$, $\Sigma_f = 8.385$, and $\Sigma_i = 0$.

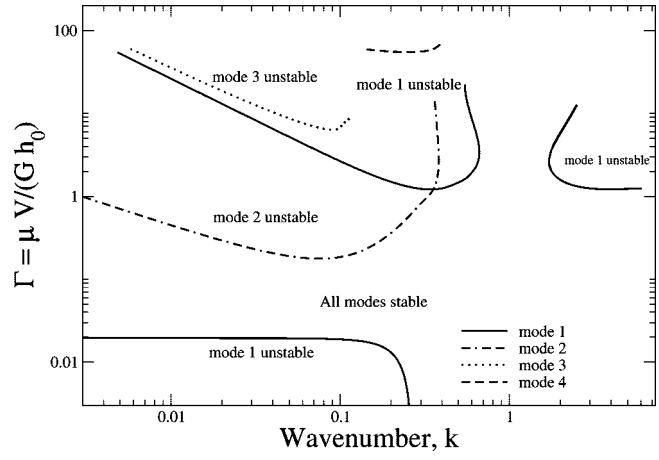

Figure 15. Neutral stability curves in $\Gamma-k$ plane for flow outside the cylinder: $Re = 0.055$, $S = 1$, $L = 2$, $\Sigma_f = 9.07$, and $\Sigma_i = 0$.

4.3. Results for Flow Inside the Cylinder. We again present the stability results in terms of a neutral stability diagram in the $\Gamma-k$ plane where stable and unstable regions are demarcated. Figure 16 presents the neutral stability diagram for $Re = 0$, $S = 5$, $L = 1$, $\Sigma_f = 4.39$, and $\Sigma_i = 2.19$. The limit of $\Gamma = 0$ is the case of a rigid cylinder where mode 1 is unstable (caused by the instability of the gas−liquid interface) for $k \leq 0.25$. As Γ is increased beyond the lower neutral curve, there is transition

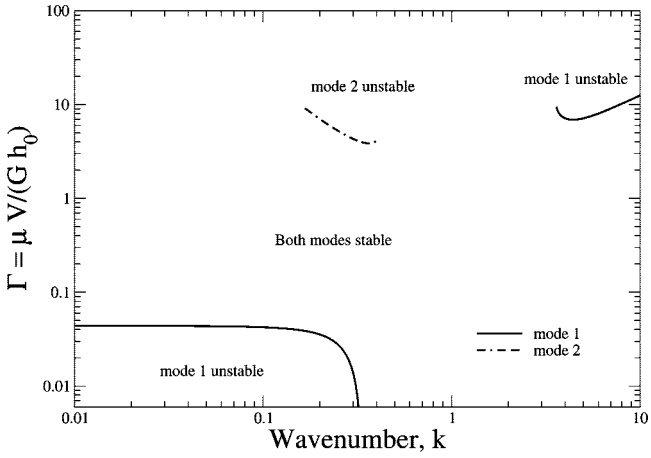

Figure 16. Neutral stability curves in $\Gamma-k$ plane for flow inside the cylinder: $Re = 0$, $S = 5$, $L = 1$, $\Sigma_f = 4.39$, and $\Sigma_i = 2.19$.

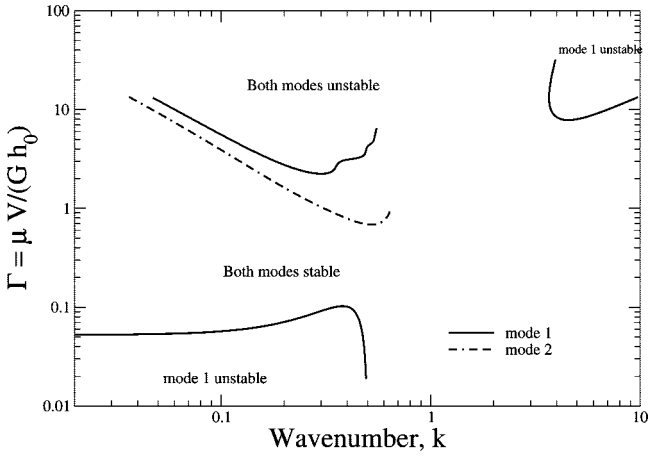

Figure 17. Neutral stability curves in $\Gamma-k$ plane for flow inside the cylinder: $Re = 0$, $S = 5$, $L = 2$, $\Sigma_f = 4.56$, and $\Sigma_i = 2.28$.

from unstable to stable perturbations of mode 1. There is large region in Γ where mode 1 is stabilized by the solid-layer deformability at all wavenumbers. As Γ is increased further, there is another neutral curve at finite k where there is a transition from stable to unstable perturbations. This instability, as we have discussed earlier, was obtained from the continuation of $Re = 0$ results, i.e., mode 2, and corresponds to the gas−liquid interface (due to mode switching). The high wavenumber instability shown by this neutral curve is because of the first normal stress difference present in the neo-Hookean solid. The most significant feature is the stability window in terms of the parameter Γ between lower and upper neutral curves, because this gap in $\Gamma-k$ plane is stable for all wavenumbers. Consequently, in this stable window, no instability must be observed experimentally. The effect of increase in thickness of the solid layer on the upper curve (at finite k) is similar to that found in the work of Shankar and Sahu[13] and Gaurav and Shankar.[14] They have demonstrated that the upper curve shifts down upon increasing the thickness L of the solid layer. A similar behavior is observed for the present case as well, when we increase the value of L from 1 to 2, which is shown in Figure 17 for $L = 2$.

In marked contrast, we observe a destabilizing effect on the lower curve upon increasing the value of L in comparison to the outside flow. The reason for the destabilization is because of the decrease in the radius of curvature (of free surface inside the tube) due to increase in the solid thickness

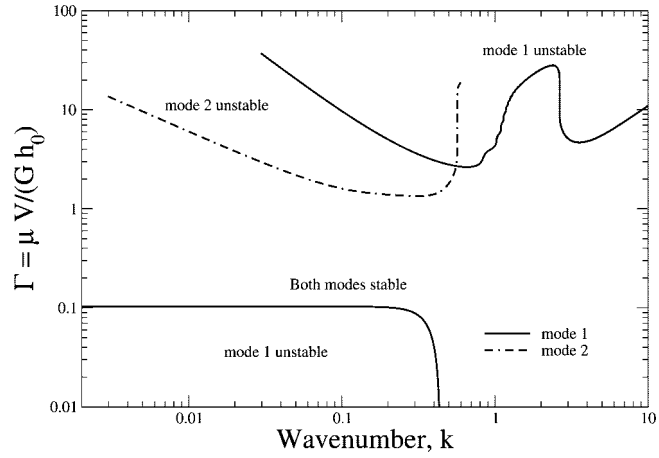

Figure 18. Neutral stability curves in $\Gamma-k$ plane for flow inside the cylinder: $Re = 0.455$, $S = 5$, $L = 1$, $\Sigma_f = 4.39$, and $\Sigma_i = 2.19$.

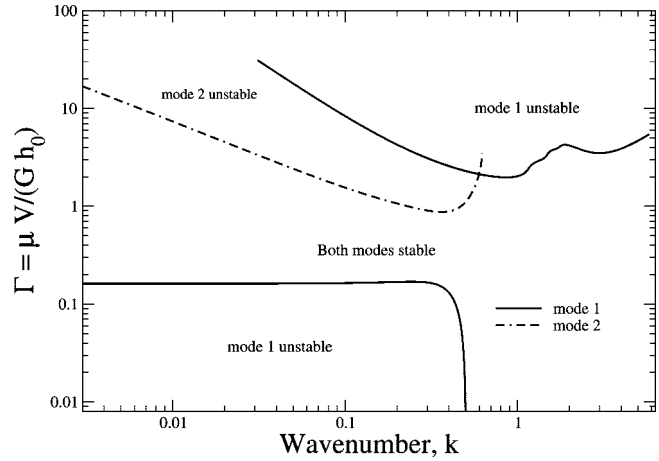

Figure 19. Neutral stability curves in $\Gamma-k$ plane for flow inside the cylinder: $Re = 0.91$, $S = 5$, $L = 1$, $\Sigma_f = 4.39$, and $\Sigma_i = 2.19$.

L, which is exactly opposite to the case of outside flow. Hence, the lower neutral curve moves up upon increasing L. By increasing the value of L from 1 to 2, the finite k mode 1 instability (caused by liquid−solid interface) appears as can be seen in Figure 17. The effect of L on the high-k instability curve is similar to the outside flow; i.e., upon increasing the value of L, the high-k neutral curve moves up. The reason for the high-k instability curve shifting up upon increasing L is similar to the explanation given above for the outside flow. The effect of increasing S on all the neutral curves is stabilizing; i.e., lower neutral curve shifts downward and the upper neutral curve shifts upward (data not shown). We next study the effect of nonzero Reynolds number on neutral stability curves. We choose the parameters $Re = 0.455$, $S = 5$, $L = 1$, $\Sigma_f = 4.39$, and $\Sigma_i = 2.19$ and show the neutral stability diagram in Figure 18. For nonzero Re, we find that the finite-k mode 1 neutral curve appears again and merges with the high-k mode 1 neutral curve. Moreover, increase in Re is destabilizing for both the modes: the lower neutral curve moves up and the upper neutral curves are move down (Figure 19). The effect of Re was found to be similar for other values of S and L probed in our numerical study (data not shown).

5. Concluding Remarks

The present study focused on the stability of the free surface in gravity-driven flow of an annular Newtonian liquid past a

soft (elastic) solid layer that is fixed outside or inside a vertical cylinder. Both low-wavenumber perturbation analysis and a numerical method were employed for this purpose. Results from the low-wavenumber analysis showed that the solid-layer deformability can suppress the capillary instability even in the creeping-flow limit at low wavenumbers. At finite *Re*, where there is an additional flow-induced inertial contribution to the free-surface instability, we showed that increase in solid deformability can still suppress the free-surface instability. At finite wavenumbers, the effect of the solid layer on the fluctuations at the gas−liquid and liquid−solid interfaces may be stabilizing or destabilizing, depending on the thickness and the shear modulus of the solid layer. At high wavenumbers, there is an additional instability due to the jump in the first normal stress difference at the (neo-Hookean) solid−liquid interface, which is stabilized by the interfacial tension at the liquid−solid interface. It was demonstrated, however, that it is possible to select the values of the thickness and shear modulus of the solid wherein there are no instabilities in the system at any wavenumber. In general, the effect of solid deformability on the stability of the two flow configurations (i.e., flow outside or inside the cylinder) is found to be largely similar. However, for a fixed radius of curvature of the tube, flow inside the cylinder becomes more unstable as compared to the flow outside the cylinder. Increase in the radius of curvature is always stabilizing for both the flow configurations, similar to the results obtained by Solorio and Sen.[11] In this study, the stability of the system was analyzed using linear stability analysis, and it was found that certain configurations which were unstable in flow past rigid surfaces can be stabilized by using a deformable solid layer. However, the linear stability analysis is limited to perturbations whose amplitudes are very small. Hence, it will be of interest in future investigations to examine whether finite amplitude perturbations can also be suppressed using a soft solid layer. Such a study would constitute a logical step further in translating the present proposition to practical applications.

Literature Cited

(1) Quere, D. Fluid coating on a fiber. *Annu. Rev. Fluid Mech.* **1999**, *31*, 347.

(2) Halpern, D.; Grotberg, J. B. Fluid-elastic instabilities in liquid-lined flexible tubes. *J. Fluid Mech.* **1992**, *244*, 615.

(3) Grotberg, J. B.; Jensen, O. E. Biofluid mechanics in flexible tubes. *Annu. Rev. Fluid Mech.* **2004**, *36*, 121.

(4) Chandrasekhar, S. *Hydrodynamic and hydromagnetic stability*; Clarendon: Oxford, UK, 1961.

(5) Drazin, P.; Reid, W. *Hydrodynamic Stability*; Cambridge University Press: Cambridge, UK, 1981.

(6) Benjamin, T. B. Wave formation in laminar flow down an inclined plane. *J. Fluid Mech.* **1957**, *2*, 554.

(7) Yih, C.-S. Stability of liquid flow down an inclined plane. *Phys. Fluids* **1963**, *6*, 321.

(8) Goren, S. L. The instability of an annular liquid thread. *J. Fluid Mech.* **1961**, *12*, 309.

(9) Lin, S. P.; Liu, W. C. Instability of film coating of wires and tubes. *AIChE J.* **1975**, *21*, 775.

(10) Krantz, W. B.; Zollars, R. L. The linear hydrodynamic stability of film flow down a vertical cylinder. *AIChE J.* **1976**, *22*, 930.

(11) Solorio, F. J.; Sen, M. Linear stability of a cylindrical falling film. *J. Fluid Mech.* **1987**, *183*, 365.

(12) Russo, M. J.; Steen, P. H. Shear stabilization of the capillary breakup of a cylindrical interface. *Phys. Fluids A* **1989**, *1*, 1926.

(13) Shankar, V.; Sahu, A. K. Suppression of instability in liquid flow down an inclined plane by a deformable solid layer. *Phys. Rev. E* **2006**, *73*, 016301 (1−12).

(14) Gaurav.; Shankar, V. Stability of gravity-driven free-surface flow past a deformable solid at zero and finite Reynolds number. *Phys. Fluids* **2007**, *19*, 024105.

(15) Gkanis, V.; Kumar, S. Instability of creeping Couette flow past a neo-Hookean solid. *Phys. Fluids* **2003**, *15*, 2864.

(16) Gkanis, V.; Kumar, S. Instability of gravity-driven free-surface flow past a deformable elastic solid. *Phys. Fluids* **2006**, *18*, 044103.

(17) Malvern, L. E. *Introduction to the Mechanics of a Continuous Medium*; Prentice-Hall: Englewood Cliffs, NJ, 1969.

(18) Holzapfel, G. A. *Nonlinear solid mechanics*; John Wiley: Chichester, UK, 2000.

(19) Macosko, C. *Rheology: Principles, Measurements, and Applications*; VCH: New York, 1994.

(20) Kelly, R. E.; Goussis, D. A.; Lin, S. P.; Hsu, F. K. The mechanism of surface wave instability in film flow down an inclinedplane. *Phys. Fluids A* **1989**, *1*, 819.

(21) Smith, M. K. The mechanism of long-wave instability in thin liquid films. *J. Fluid Mech.* **1990**, *217*, 469.

(22) Kumaran, V.; Fredrickson, G. H.; Pincus, P. Flow induced instability of the interface between a fluid and a gel at low Reynolds number. *J. Phys. II France* **1994**, *4*, 893.

Received for review December 27, 2007
Revised manuscript received May 7, 2008
Accepted May 16, 2008

IE701771M